Insights into the Mechanism of *Escherichia coli* Methionine Aminopeptidase from the Structural Analysis of Reaction Products and Phosphorus-Based Transition-State Analogues[†,‡]

W. Todd Lowther,[§] Yan Zhang,[§] Peter B. Sampson,[||] John F. Honek,[||] and Brian W. Matthews*[,§]

Institute of Molecular Biology, Howard Hughes Medical Institute and Department of Physics, 1229 University of Oregon, Eugene, Oregon 97403, Department of Chemistry, University of Waterloo, Waterloo, Ontario, Canada N2L 3G1

Received July 23, 1999; Revised Manuscript Received September 17, 1999

ABSTRACT: In an effort to differentiate between alternative mechanistic schemes that have been postulated for *Escherichia coli* methionine aminopeptidase (eMetAP), the modes of binding of a series of products and phosphorus-based transition-state analogues were determined by X-ray crystallography. Methionine phosphonate, norleucine phosphonate, and methionine phosphinate bind with the N-terminal group interacting with Co2 and with the respective phosphorus oxygens binding between the metals, interacting in a bifurcated manner with Co1 and His178 and hydrogen bonded to His79. In contrast, the reaction product methionine and its analogue trifluoromethionine lose interactions with Co1 and His79. The interactions with the transition-state analogues are, in general, very similar to those seen previously for the complex of the enzyme with a bestatin-based inhibitor. The mode of interaction of His79 is, however, different. In the case of the bestatin-based inhibitor, His79 interacts with atoms in the peptide bond between the P_1' and P_2' residues. In the present transition-state analogues, however, the histidine moves 1.2 Å toward the metal center and hydrogen bonds with the atom that corresponds to the nitrogen of the scissile peptide bond (i.e., between the P_1 and P_1' residues). These observations tend to support one of the mechanistic schemes for eMetAP considered before, although with a revision in the role played by His79. The results also suggest parallels between the mechanism of action of methionine aminopeptidase and other "pita-bread" enzymes including aminopeptidase P and creatinase.

Methionine aminopeptidases (MetAPs)[1] remove the initiator N-terminal methionine residue of proteins and peptides of at least three residues in length (*1*). The physical characteristics of the active site, however, restrict enzymatic action to substrates containing a small and uncharged residue at the penultimate position (*1*−*3* and references therein). The removal of methionine represents a critical step in the maturation of proteins for proper function, targeting, and eventual degradation (*3*−*5*). The physiological importance of MetAP activity is underscored by the lethality of the deletion or inhibition of all MetAP genes or gene products in *Escherichia coli*, *Salmonella typhimurium*, and *Saccharomyces cerevisiae* (*6*−*8*). Moreover, MetAPs have been shown biochemically and structurally to be the molecular target of the anti-angiogenesis agent fumagillin and its derivatives (*9*−*13*). These observations suggest that a better understanding of the catalytic mechanism and substrate specificity of MetAPs will be useful in the development of therapeutics for preventing the vascularization of tumors and the treatment of microbial and fungal infections (*6*, *8*, *14*, *15*).

The analysis of the high-resolution crystal structures of the native enzyme and of a bestatin-based inhibitor complex, coupled with mutational analysis of His79 and His178, suggested two potential reaction mechanisms (*16*, *17*). The main difference between these mechanisms and their associated transition states (Figure 1) is in the location of the carbonyl oxygen atom (O_C) of the substrate upon binding. In mechanism I, this atom is proposed to interact with Glu204, a conserved metal ligand. This interaction could facilitate the simultaneous transfer of a proton to O_C together with the attack of the scissile bond by the metal-bridging μ-hydroxide or water nucleophile (O_N) leading to the formation and stabilization of a tetrahedral intermediate. In mechanism II, the O_C atom was proposed to be oriented in a different direction so as to interact with Co1 and His178. In this scheme, the proximity of Glu204 to the nitrogen atom of the scissile bond suggested that Glu204 might shuttle a proton from the attacking μ-hydroxide to the new N-terminus. In these reaction schemes, His178 could play two different roles, either to act as a proton donor to the leaving group

[†] This work was supported in part by the National Research Service Award F32-GM17536 (W.T.L.) and Research Grant GM20066 (B.W.M.) from the National Institutes of Health. P.B.S. and J.F.H. were supported by the NSERC (Canada).

[‡] The coordinates have been deposited in the Protein Data Bank under the accession numbers 1C21, 1C22, 1C23, 1C24, 1C27.

* To whom correspondence should be addressed. E-mail: brian@uoxray.uoregon.edu. Phone: 541-346-2572. Fax: 541-346-5870.

[§] University of Oregon.

[||] University of Waterloo.

[1] Abbreviations: MetAP, methionine aminopeptidase; eMetAP, *E. coli* MetAP; creatinase, creatine amidinohydrolase; AMPP, aminopeptidase P; TFM, L-trifluoromethionine; MetP, 1-amino-3-(methylmercapto)propylphosphonic acid; MetI, 1-amino-3-(methylmercapto)-propylphosphinic acid; NleP, norleucine phosphonic acid; AHHpA, (3*R*)-amino-(2*S*)-hydroxyheptanoic acid.

10.1021/bi991711g CCC: $18.00
Published on Web 10/21/1999

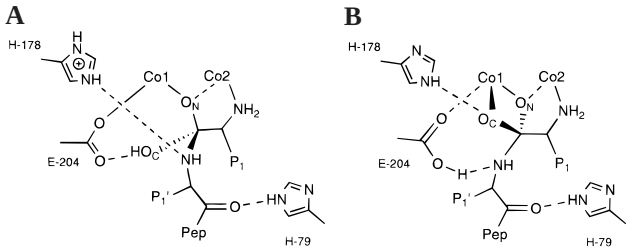

FIGURE 1: Alternative models for the transition state in MetAP catalysis as proposed by Lowther et al. (*17*). The oxygen atoms are labeled according to their proposed origin: O_N, attacking nucleophile; O_C, the substrate carbonyl oxygen. (A) Model in which the transition state is stabilized by interactions with Glu204 and the metal center. (B) Model in which the intermediate is stabilized by the chelation of Co1 and hydrogen bonding with His178. His79 interacts with the backbone P_1' carbonyl in both schemes. Nomenclature of Schechter and Berger (*18*).

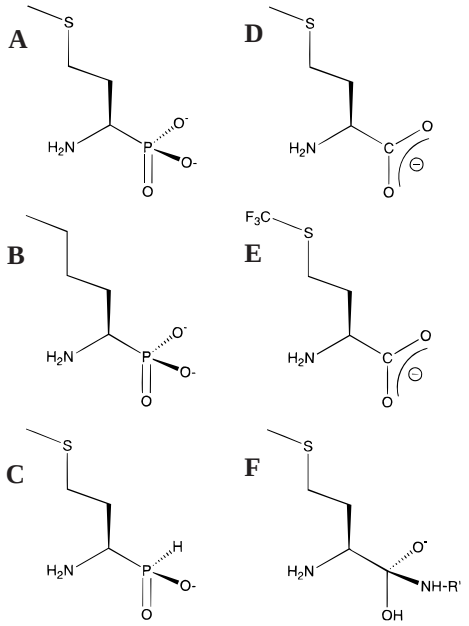

FIGURE 2: Reaction product and transition-state analogues of MetAP: (A) L-methionine phosphonate (MetP), (B) L-norleucine phosphonate (NleP); (C) L-methionine phosphinate (MetI); (D) L-methionine; (E) L-trifluoromethionine (TFM); (F) the putative *gem*-diolate transition state.

(mechanism I) or to ameliorate the stabilization of the carboxy anion of the tetrahedral intermediate by Co1 (mechanism II). The significant residual activity of the His178Ala mutant, however, demonstrated that the contribution of His178, whatever it might be, was not critical for catalysis. In both mechanisms, His79 was proposed to help orient the substrate in a productive manner for catalysis via a hydrogen bond to the carbonyl oxygen of the penultimate residue (Figure 1). The nearly complete loss of activity of the His79Ala mutant suggested that this interaction, though remote from the scissile bond, was crucial for catalysis. A rather different mechanistic scenario has also been proposed by Liu and co-workers (*11*) based on the mode of inhibition of human MetAP II by fumagillin and ovalicin.

In an effort to clarify the reaction coordinate of eMetAP, the binding mode of several reaction products together with phosphorus-containing transition-state analogues (Figure 2) were determined by X-ray crystallography. Comparisons of the present results with the previously studied bestatin-based inhibitor (*17*) and the Pro-Leu product complex of AMPP (*19*) favor one of the reaction pathways proposed previously and suggest a potential alternative role for His79.

MATERIALS AND METHODS

Reaction Product and Transition-State Analogue Syntheses. L-Met was purchased from Sigma. L-Trifluoromethionine [L-*S*-(trifluoromethyl)homocysteine; TFM] was synthesized as previously described (*20*, *21*). NMR spectra of synthetic compounds were recorded on a Bruker AM-250 spectrometer, operating at 250 MHz for ^{1}H and 62.5 MHz for ^{13}C. Chemical shifts are reported downfield from TMS ($\delta = 0$ ppm) for ^{1}H NMR in $CDCl_3$ solution and TSP [(3-trimethylsilyl)-1-propanesulfonic acid sodium salt] for samples in D_2O. For ^{13}C NMR spectra, chemical shifts are reported relative to the central $CDCl_3$ resonance ($\delta = 77.0$ ppm). ^{31}P NMR spectra were recorded on a Bruker AC-200 spectrometer operating at 80.0 MHz. Chemical shifts are reported downfield from H_3PO_4 ($\delta = 0$ ppm). HPLC separations were performed using a reversed phase μ-Bondapak C-18 column (25 × 100 mm) (Waters, Inc.).

The methionine analogues, 1-amino-3-(methylmercapto)-propylphosphonic acid (MetP) and 1-amino-3-(methylmercapto)propylphosphinic acid (MetI), were prepared according to the methods of Kudzin and Stec (*22*) and Baylis et al. (*23*), respectively. Both compounds were purified to homogeneity by HPLC (retention times in H_2O/0.1% TFA: 14 min at 4 mL/min for both compounds). The norleucine analogue, norleucine phosphonic acid (NleP), was prepared by alkylation of the lithium anion of diethyl [(diphenylmethyleneamino)methyl]phosphonate with *n*-butyl iodide (*24*). Hydrolysis of the diethyl ester and Schiff base with 48% aqueous HBr/AcOH gave the aminophosphonic acid as a crude salt. The free acid was isolated by precipitation with propylene oxide. The syntheses of all phosphorus-containing analogues resulted in a racemic mixture at the C^α carbon (both L- and D-forms of the amino acid).

(1) (D,L)-Diethyl-1-[(diphenylmethyleneamino)methyl]-pentylphosphonate. To a stirred solution of lithium diisopropylamide (0.33 mmol) in anhydrous THF, a solution of diethyl[(diphenylmethyleneamino)methyl]phosphonate (*24*) (100 mg, 0.3 mmol) in THF (1 mL) was added at −78 °C under argon atmosphere. The resulting dark orange solution was stirred for 30 min. A solution of *n*-butyl iodide (0.33 mmol, 38 mL) in THF (1 mL) was then added and the mixture stirred at −78 °C for 4 h. The light orange solution was warmed to room temperature and saturated aqueous NH_4Cl (2 mL) was added. The mixture was extracted with ethyl acetate (3 × 15 mL), and the combined organic fractions were washed with water (2 × 10 mL), dried over $MgSO_4$, and concentrated in vacuo. The resulting orange oil (105 mg, 91%) was used in the next reaction without further purification. Compound characteristics: IR ($CHCl_3$) 1619 cm^{-1} (C═N), 1242 cm^{-1} (P═O); ^{1}H NMR ($CDCl_3$) 7.64 (d, 2 H, J = 6.4 Hz), 7.22−7.56 (m, 8H), 4.03−4.24 (m, 4H), 3.86 (dt, 1H, J = 10.1 Hz, 3.3 Hz), 1.83−2.04 (m, 2H), 1.15−1.35 (m, 4H), 1.33 (t, 3H, J = 7.0 Hz), 1.31 (t, 3H, J = 7.0 Hz) 0.83 (t, 3H, J = 7.3 Hz); ^{13}C NMR δ 161 (*C*═N), 136.1, 130.0, 128.4, 128.0 (arene), 62.2 (d, J_{POCC} = 5.8 Hz $POCH_2$), 61.6 (d, J_{PC} = 159 Hz, *C*H) 30.6, 28.7, 22.3, 16.4 (d, J_{POC} = 5.7 Hz, $POCH_2CH_3$) 13.8; ^{31}P NMR δ 25.3.

(2) (D,L)-1-Aminopentylphosphonate. A mixture of diethyl-1-[(diphenylmethyleneamino)methyl]pentylphosphonate (100

Table 1: X-ray Data Collection and Refinement Statistics[a]

	MetP	MetI	NleP	Met	TFM
cell parameters					
a (Å)	39.2	39.3	39.3	39.2	39.2
b (Å)	67.5	67.6	67.2	67.6	67.6
c (Å)	48.8	48.9	49.1	48.9	48.8
β (deg)	111.2	111.2	111.5	111.2	111.1
X-ray data collection					
resolution range (Å)	32.2−2.0	24.6−1.7	36.6−1.95	24.8−1.8	27.1−1.75
collected reflections	79 515	126 529	68 595	85 232	116 107
unique reflections	16 137	26 200	16 281	21 097	24 021
completeness (%)	99.8 (100)	99.6 (99.8)	93.6 (88.6)	95.1 (90.2)	99.9 (100)
$<I/\sigma(I)>$	27.4 (6.4)	38.9 (4.4)	28.8 (4.6)	35.2 (4.4)	35.4 (4.5)
R_{sym} (%)	6.4 (20.0)	4.4 (27.4)	5.6 (26.7)	4.5 (25.6)	4.9 (26.4)
refinement statistics					
R (%)	15.1	16.4	17.0	16.3	16.3
Δ_{bonds} (Å)	0.011	0.010	0.011	0.010	0.011
Δ_{angles} (deg)	2.16	2.01	2.10	2.05	2.10
$\Delta_{trig\ planes}$ (Å)	0.009	0.007	0.007	0.006	0.009
Δ_{planes} (Å)	0.012	0.012	0.012	0.012	0.013
thermal factors					
protein atoms (Å^2)	20.6	22.9	26.5	24.6	21.4
solvent atoms (Å^2)	29.9	33.3	33.9	34.7	32.2
ligand atoms (Å^2)	17.6	25.0	33.7	39.0	32.0
Co1, Co2 (Å^2)	15.5, 15.6	17.6, 16.1	23.8, 24.0	20.4, 21.6	15.5, 15.1
Na^+ (Å^2)	12.1	14.3	27.5	11.8	9.5

[a] The holoenzyme crystallizes in space group $P2_1$ with cell dimensions $a = 39.3$ Å, $b = 67.7$ Å, $c = 48.9$ Å, $\beta = 111.2°$ (*17*). $<I/\sigma(I)>$ is the root-mean-square value of the intensity measurements divided by their estimated standard deviation. R_{sym} gives the average agreement between the independently measured intensities. The values for the highest resolution shells are given in parentheses: MetP (2.00−2.07 Å), MetI (1.70−1.76 Å), NleP (1.95−2.02 Å), Met (1.80−1.86 Å), TFM (1.75−1.81 Å). R is the crystallographic residual following refinement. Δ_{bonds}, Δ_{angles}, $\Delta_{trig\ planes}$, and Δ_{planes} give the average departure from ideal values of the bond lengths, bond angles, trigonal planes, and other planar groups of atoms.

mg, 0.26 mmol) and concentrated HCl/AcOH 1:1 (3 mL) was refluxed (16 h) and cooled to room temperature. Water (10 mL) was added, and the mixture washed with toluene (2 × 15 mL). The aqueous layer was concentrated to dryness and dissolved in anhydrous ethanol (2 mL). Propylene oxide was added until a pH of 6 was achieved. The slightly yellow residue was purified by HPLC (retention time in H_2O/0.1% TFA: 15 min at 4 mL/min) to give (20 mg, 46%) of a white powder. Compound characteristics: mp (uncorrected) 249−251 °C; ^{1}H NMR (D_2O) d 3.35 (m, 1H), 1.81−2.04 (m, 1H), 1.60−1.79 (m, 1H), 1.29−1.55 (m, 4H), 0.90 (t, 3H, J = 7.3 Hz); ^{13}C NMR δ 48.8 (d, J_{PC} = 147 Hz, *C*HP), 27.7 (d, J_{PCC} = 9 Hz, PCH*C*H$_2$) 27.5, 21.7, 13.1; ^{31}P NMR d 16.5.

Crystallization, Data Collection, and Refinement. Recombinant eMetAP (R175Q) was prepared and crystallized as previously reported (*9*, *17*). Briefly, crystals of the Co(II)-substituted enzyme were grown at room temperature by vapor diffusion in 20−30 μL sitting drops after mixing the protein [12 mg/mL, 25 mM Hepes, pH 6.8, 25 mM K_2SO_4, 100 mM NaCl, 1 mM $CoCl_2$, 15 mM methionine, and 48.8 mM *N*-octanoyl sucrose (Calbiochem-Novabiochem Corp., La Jolla, CA)] 1:1 with well solutions containing 24−26% PEG 4000, 0.1 M Hepes, pH 7.0−7.2, and fresh 2 mM $CoCl_2$. Crystals were transferred to 50 mM Hepes, pH 7.0−7.1, 1 mM fresh $CoCl_2$, 28−29% PEG 4000 containing the following compounds with the concentration used and the soak time prior to data collection as indicated: MetP (saturated solution, ∼25 mM, 3 h), MetI (200 mM, 4 h), NleP (25 mM, 3 h), Met (saturated solution, >16 h), TFM (40 mM, >16 h).

X-ray diffraction data were collected at room temperature by the oscillation method on an R-Axis IV with a Rigaku rotating anode source. The raw data were merged and scaled using DENZO and SCALEPACK (*25*). The coordinates of the native structure were used as the starting model (*17*). Following rigid-body refinement initially using the entire model without the cobalt atoms and subsequently with 20 smaller secondary structural elements, the model was improved by the iterative addition of water molecules to 3σ positive difference features in an $F_o - F_c$ electron density map and the modification of side-chain positions using the programs CHAIN (*26*) or O (*27*). The model was refined with TNT after each session of building (*28*). Models for the bound ligands were added when the electron densities for their placement were unequivocal. Expected bond lengths and angles for the different methionine and transition-state analogues were determined using the BUILDER and DISCOVER programs in the InsightII package (Biosym Technologies, San Diego/Molecular Simulations, Waltham, MA). At the final stages of building, all models, except for the MetI complex, were refined with unit occupancy and correlated thermal factor restraints (*29*). The MetI complex (1.7 Å) was refined without thermal factor restraints and the occupancies for two alternative conformations of the inhibitor were estimated. Atomic coordinates were superimposed with the SUPERIMPOSE program in the InsightII package. Figures 3−6 were generated with BOBSCRIPT (*30*) or MOLSCRIPT (*31*).

RESULTS

The binding modes of the reaction products and transition-state analogues shown in Figure 2 were determined by X-ray crystallography after soaking pregrown crystals (*17*) in synthetic mother liquor solutions containing millimolar concentrations of the different ligands (see Materials and Methods). The maximum resolution of the data ranged from

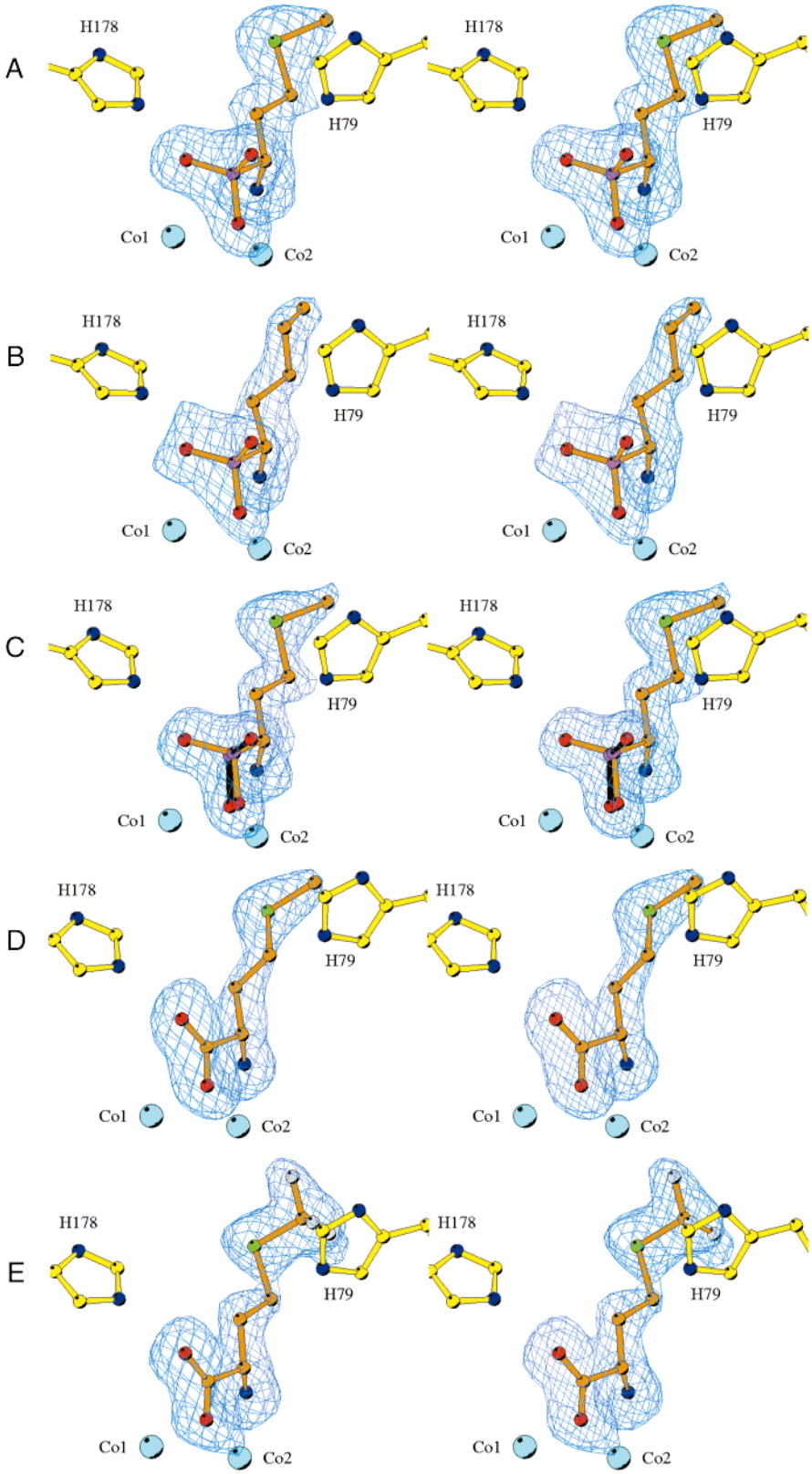

FIGURE 3: eMetAP−ligand complexes. Each stereo figure shows the positive blue contours of the "omit" $F_o - F_c$ electron density maps for each complex calculated to the highest possible resolution (Table 1). The displayed ligand atoms were omitted from the refined model during map calculation (see Materials and Methods). Each map was contoured at 3σ where σ is the root-mean-square value of the electron density through the unit cell. Color scheme for atoms: red, oxygen; blue, nitrogen; magenta, phosphorus; yellow, carbon atoms for eMetAP; orange, carbon atoms for the different ligands; cyan, cobalt; fluorine, white. (A) L-MetP; (B) L-NleP; (C) L-MetI with an alternative conformation shown in black (see text); (D) L-Met; (E) L-TFM.

1.7 Å to 2.0 Å with the final models having crystallographic *R* factors from 15.1 to 17.0% and acceptable geometry (Table 1).

Phosphonate and Phosphinate Transition-State Analogues. MetP, NleP, and MetI were synthesized to mimic the putative tetrahedral intermediate of the reaction (Figure 2F). Specif-

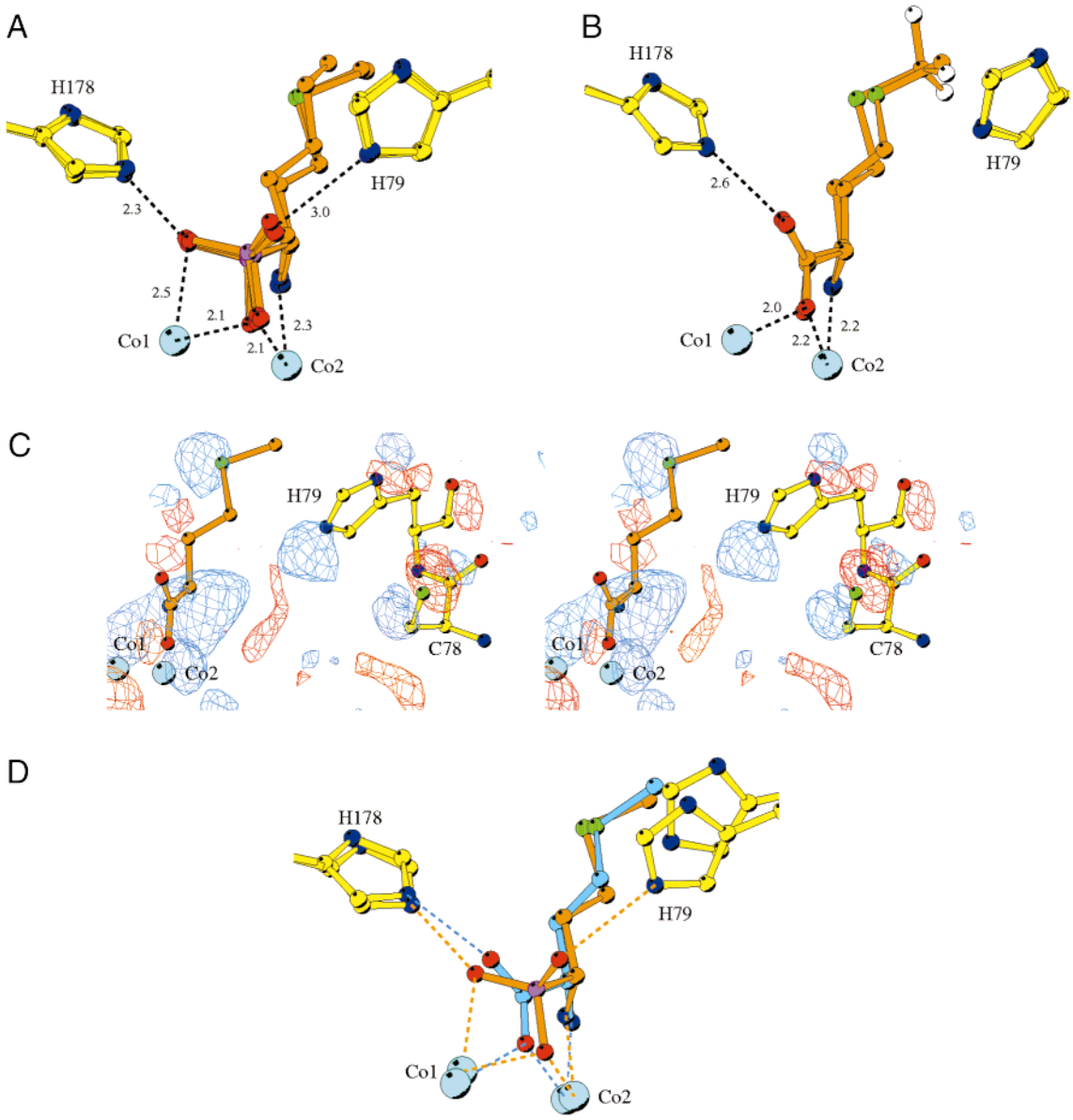

FIGURE 4: Comparison of different ligands (Figure 2) bound to eMetAP. (A) Superposition of the phosphorus-containing transition-state analogues, MetP, MetI, and NleP. (B) Superposition of the reaction product Met and its analogue TFM. In panels A and B the C^{α} carbons of MetAP for each complex were brought to a common frame of reference by aligning them with the bestatin-based inhibitor complex (*17*). The RMS discrepancy for the superpositions ranged 0.29−0.38 Å. The dashed black lines indicate the interatomic distances (Å) for MetP (panel A) and Met (panel B). The distance between Co1 and Co2 is 3.2 Å. The same color scheme is used as in Figure 3 except that the alternative conformations of MetI are both shown in orange. (C) Electron density map with coefficients ($F_{MetP} - F_{Met}$) contoured at 5σ: blue, positive; red, negative. The map was calculated to 2.0 Å resolution using the complex of eMetAP with methionine as the reference structure, but with the ligand omitted. Positive density near the metal center indicates the extra phosphorus and oxygen atoms of the phosphonate analogue. The compensating positive-negative features around Cys78 and His79 illustrate the movement of His79 toward the metal center. (D) Comparison of the mode of binding of Met (blue carbon atoms) and MetP (orange carbon atoms).

ically, these analogues exhibit features representative of the carbonyl group and the amide nitrogen atom of the scissile peptide bond. The synthetic strategy produced a mixture of both enantiomers. Even though crystals were soaked with racemic mixtures of the ligand, in each case the electron density (Figure 3, panels A−C) was consistent with only the physiological (L) configuration. The analogues bind to the active site in a similar manner (Figure 4A), all displaying N-terminal ligation to Co2, a bridging coordination between Co1 and Co2, a bifurcated interaction between Co2 and His178, and a hydrogen bond (3.0 Å) with His79. During refinement of the MetI complex, it was initially unclear whether the oxygen atoms bound in two or more conformations or that MetI might have been enzymatically converted to MetP. Mass spectroscopic analysis (data not shown) of MetI incubated in water, buffer, and synthetic crystallization mother liquor with and without enzyme showed the ligand to be completely stable. Stemming from these results, MetI was modeled to bridge between the cobalt ions and to interact with either His178 or His79 (Figure 3C). During the final stages of the refinement, the occupancies of the phosphinate groups were allowed to vary independently and resulted in values of 0.6 and 0.7. The third possible orientation in which the oxygen atoms interact with His79 and His178 was not included. This binding mode seems less likely since it does not include an interaction with either metal ion, but cannot be completely ruled out.

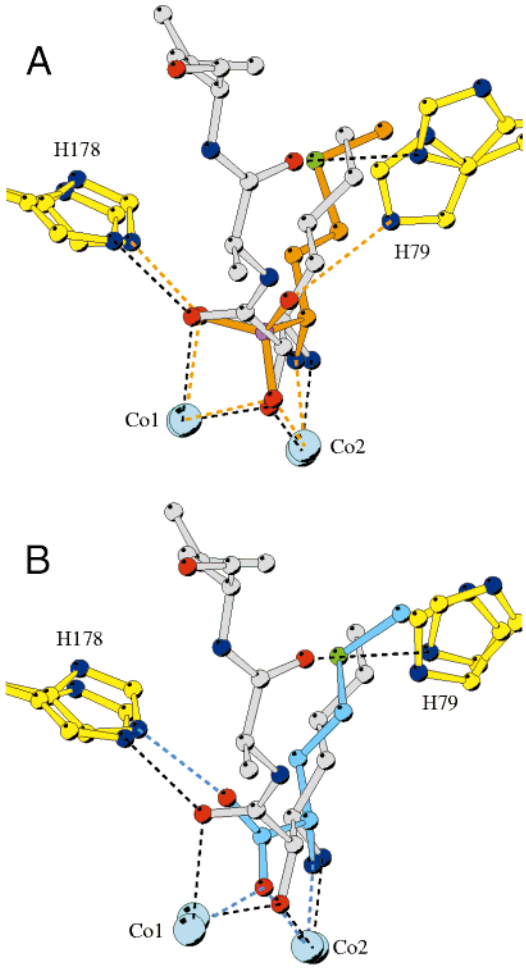

FIGURE 5: (A) Comparison of the bestatin-based inhibitor AHHpA-Ala-Leu-Val-Phe-OMe (gray atoms, black dashed lines) with MetP (orange atoms and orange dashed lines). (B) Comparison of the binding to eMetAP of methionine (blue atoms and blue dashed lines) and the bestatin-based inhibitor (gray carbon atoms and black dashed lines). Only the first three residues of the latter inhibitor could be seen in the electron density map (*17*).

Methionine and Trifluoromethionine. Methionine and its analogue trifluoromethionine (TFM) were used to investigate how product binds to the metal center of the enzyme. The synthetic strategy for TFM, in contrast to the phosphorus-containing analogues, yielded only the (L) enantiomer. Both compounds bind to the active site in a similar manner (Figures 3, panels D and E, and 4B) having the same N-terminal and metal-bridging interactions as MetP, NleP, and MetI. However, in contrast to the tetrahedral phosphorus-containing compounds, the planar carboxyl group results in a longer interaction with His178 (2.6 Å) and has a single interaction with Co1. The loss of an interaction with Co1 suggests that the coordination number of this metal ion decreases as the product is formed.

His79 Movement toward the Metal Center. A comparison of the MetP and the Met complexes (Figure 4, panels A and B) reveals that the protein structure responds differently in binding the two types of ligand. In the phosphonate and the phosphinate structures, His79 moves 1.2 Å toward the metal center to establish a hydrogen bond (3.0 Å) with one of the oxygen atoms (Figure 4, panels C and D). This oxygen atom mimics the location of the nitrogen atom of the scissile peptide bond. The movement of His79 is part of a larger regional shift in the enzyme in which the extended loop containing residues 75−81, as well as residues 216−223 move toward the metal site to generate a "closed" conformation.

DISCUSSION

The binding of the bestatin-based inhibitor (3*R*)-amino-(2*S*)-hydroxyheptanoyl-L-Ala-L-Leu-L-Val-L-Phe-OMe (*17*) suggested the mode of binding of substrates to eMetAP. Though this complex explained the substrate specificity of the enzyme and identified key metal interactions, questions remained concerning the catalytic mechanism. The metal center was proposed to facilitate the activation of the nucleophile and to provide binding determinants for the proper docking of the N-terminal methionine. It was less apparent, however, whether the oxygen atom of the scissile peptide bond bound directly to Co1 of the metal center or to the free $O^{\epsilon 2}$ atom of the metal ligand Glu204 (Figure 1). The present analysis of product and phosphorus-containing transition-state analogues helps resolve this question and gives additional insights into the functions of the metal center and of His79 and His178.

Comparisons with the Bestatin-Based Inhibitor. The active-site interactions of the product and transition-state analogues determined here are similar to that previously observed for the substrate-like bestatin-based inhibitor (*17*). While the N-terminus is bound to Co2 in all cases, differences are observed in the location of the atoms that mimic the transition state or represent the scissile peptide bond. The phosphorus-containing compounds and the bestatin-based inhibitor interact with both metals (Figure 5A). Met and TFM, however, lose one interaction with Co1 (Figure 5B). Another difference relative to the bestatin-based inhibitor is that the product and transition-state analogues bind in the physiological (L) conformation. Notwithstanding the resultant changes in the positions of the N-terminal amino group and the C^{α} carbon atom, the side-chain atoms interact with the S_1 hydrophobic pocket (His79, Cys59, Cys70, Tyr62, Tyr65, Phe177, and Trp221) in a comparable manner.

A superposition of the MetP complex on the bestatin-based complex also shows a substantial movement of His79 (Figure 5A). This movement could correspond to an adjustment that occurs during catalysis or might be a consequence of the enzyme neutralizing the additional negative charge on the phosphate group or could also reflect the lack of additional C-terminal structural elements present in an extended substrate. In contrast to the phosphorus analogues, the "frameshift" introduced by the amino-hydroxyheptanoyl (AHHpA) moiety permits the P_1' carbonyl group to bind to the enzyme without a significant change in conformation. This may contribute to the potency of this inhibitor (*32*). While these observed differences in binding may suggest that the "true" interactions with His79 during catalysis are yet to be observed crystallographically, a comparison with the product complex of the homologous enzyme aminopeptidase P supports the notion that His79 does interact with the nitrogen atom of the scissile peptide bond.

Comparison with the Pro−Leu Complex of Aminopeptidase P. Aminopeptidase P (AMPP) preferentially removes the N-terminal residue of substrates with Xaa−Pro bonds (*33*). Despite the differences in substrate specificity, sequence

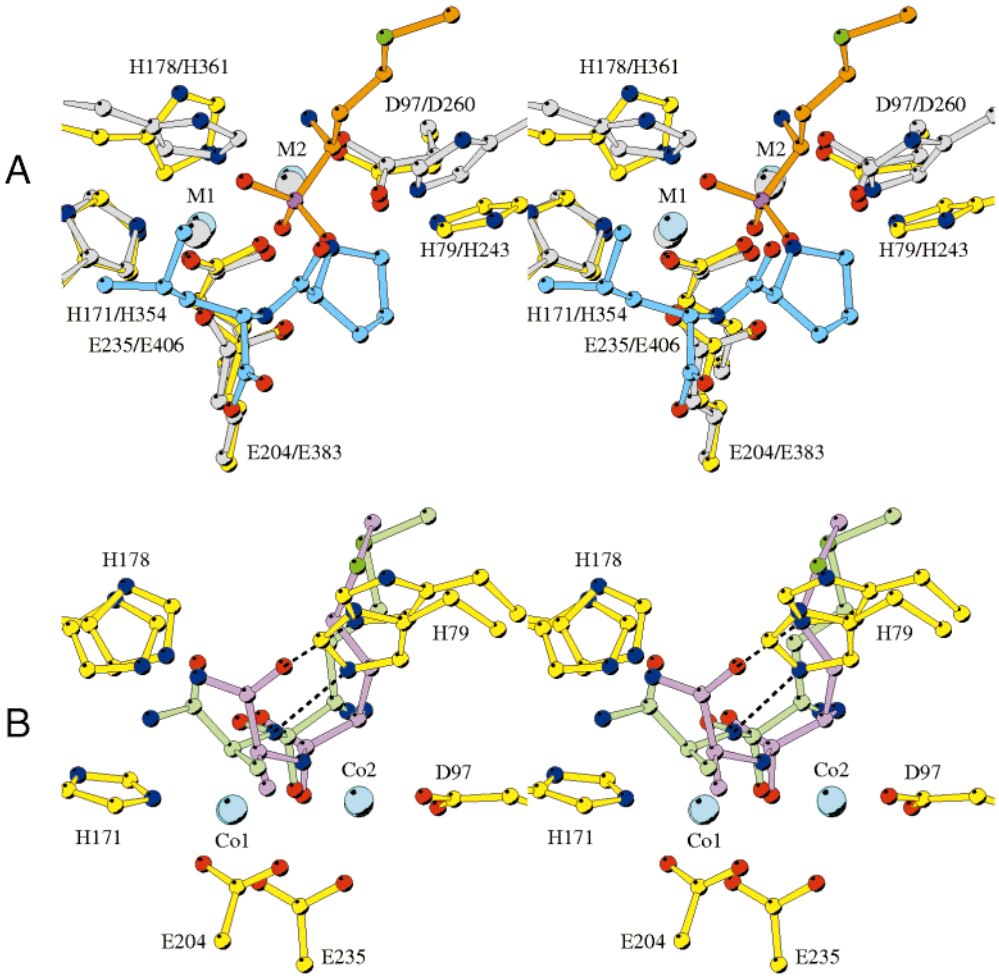

FIGURE 6: (A) Comparison of the MetP-eMetAP complex with the C-terminal product complex, Pro-Leu, of AMPP (*19*; PDB accession code 1A16). The two models were superimposed using the coordinates of all the atoms constituting the metal center and the conserved histidine residues His79/His243 and His178/His361 (RMS 0.75 Å). Asp108/Asp271 are not shown for clarity. The atom labels indicate the eMetAP/AMPP residues. Carbon atom coloring scheme: yellow, eMetAP; orange, MetP; gray, AMPP; light blue, Pro-Leu. The metal atoms, M1 and M2, are Co(II) (cyan) for eMetAP and Mn(II) for AMPP (also colored gray). (B) Comparison of the transition state model for eMetAP as based on the bestatin-based inhibitor complex (pink carbon atoms) (*17*) and as modified (light green carbon atoms) following the determination of the structures described herein. The models are truncated at the P_2' nitrogen atom for clarity. MetAP does not cleave dipeptide substrates (*1*). The dotted lines illustrate the difference in the mode of interaction of His79, this being the key difference between the two models.

alignments and structural comparisons have shown that not only AMPP but also prolidase and creatinase share the same "pita-bread" fold in the catalytic domain as MetAPs (*19*, *34*, *35*). A superposition of the C-terminal product complex of AMPP and the MetP−eMetAP complex (Figure 6A) shows that the position of the N-terminal nitrogen atom of Pro-Leu, originally part of the scissile bond, corresponds to the third oxygen atom of MetP. This nitrogen atom makes a long hydrogen bond with His243 (3.2 Å), analogous to the hydrogen bond (3.0 Å) between the oxygen of MetP and His79 in eMetAP (Figure 4A). Yet another analogous interaction is observed between the His79 equivalent, His232, in creatinase (*34*; Figure 8 in ref *17*). In this case, the hydrogen bond (3.0 Å) is to the nitrogen atom of the guanidinium group of carbamyl sarcosine, which is reminiscent of a peptide bond. These observations suggest that the movement of His79, or its equivalent in creatinase and AMPP, to establish a hydrogen bond to the backbone of the substrate may be a critical component of catalysis.

Revised Transition-State Model. The new information from the product and transition-state analogues, together with the previously determined structures of the native and inhibited forms of eMetAP, and comparisons with creatinase and AMPP, suggest a revision in the previously proposed model for the transition state. The revised model (Figure 6B) was constructed using the following assumptions: (i) the N-terminus of the substrate coordinates to Co2 at the expense of a terminal solvent molecule, (ii) a noncovalent *gem*-diolate tetrahedral intermediate is formed after attack by the metal-bridging water or hydroxide nucleophile (O_N), (iii) the original carbonyl oxygen (O_C) of the scissile peptide bond interacts with Co2 and His178 as observed for the MetP, NleP, and MetI analogues, and (iv) His79 makes a hydrogen-bonding interaction with the nitrogen of the scissile peptide bond.

The new model (Figure 6B) is very similar to that proposed before for mechanism II (*17*) except for the substrate backbone interactions to His79. On the basis of the bestatin-derived complex, His79 was thought to interact with the carbonyl oxygen atom of the penultimate residue, but the newer results suggest that it could move to hydrogen bond directly to the scissile nitrogen. The absence of any interac-

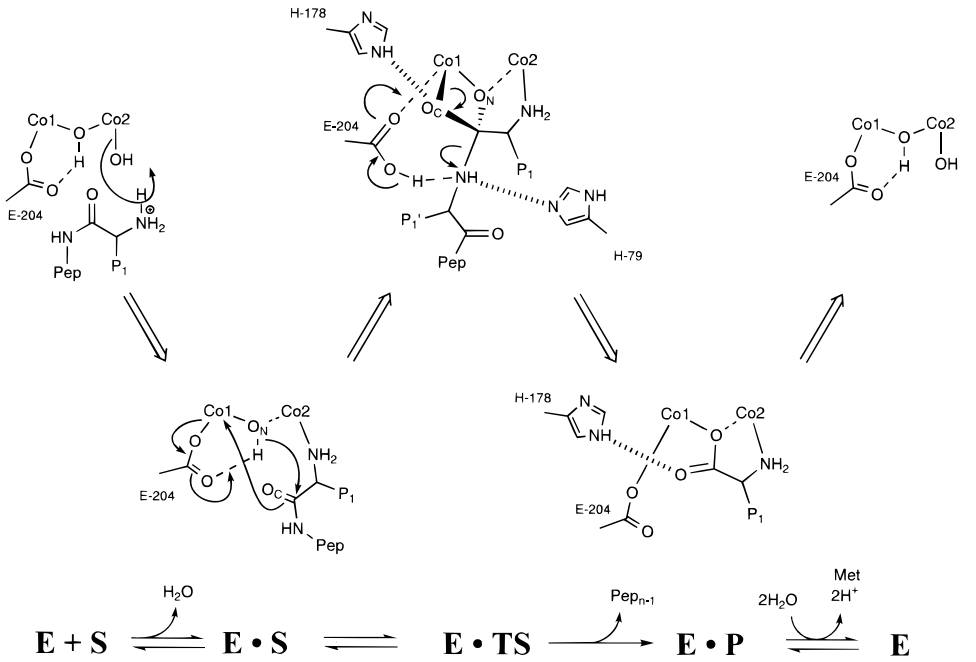

FIGURE 7: Proposed reaction mechanism for eMetAP. O_N and O_C correspond, respectively, to the oxygen atom of the nucleophile and the carbonyl oxygen of the scissile bond. Dashed and solid lines indicate interactions with the ligands or metals of the di-Co(II) center. Hashed lines indicate hydrogen bonding interactions (see Discussion).

tions with Glu204 by Met or TFM suggests that catalysis via mechanism I is less likely.

On the basis of the demonstration that His231 of human MetAP-II (the counterpart of His79 of eMetAP) is covalently modified by the inhibitors fumagillin and ovalicin, Griffith et al. (*11*) proposed a mechanism of action for the human enzyme in which His231 acts as a general base to promote the attack of a metal-bound water molecule on the substrate. The geometry of the active site, as seen in the *E. coli* enzyme, does not obviously support this proposal. In the first place, the substrate appears to interpose itself between His79 and the dinuclear center (e.g., see Figure 4A). In the second place, His79 seems to be too far away from the metal-bridging solvent molecule. (In the MetP complex, the distance from $N^{\epsilon 2}$ of His79 to this site is 5.1 Å; in the Met complex it is 6.3 Å.) Thus, a mechanism for eMetAP akin to that proposed by Griffith et al. (*11*) for the human enzyme would require a quite substantial rearrangement of elements of the active site.

Mechanism of Catalysis. The mechanism by which MetAP appears to affect hydrolysis of the peptide bond between the N-terminal methionine and penultimate residue is summarized in Figure 7. Binding of the substrate, which includes direct interactions with both metals, leads to an expansion of the coordination sphere of Co1 from five to six. This alteration in the electronic character of the dinuclear center may activate the μ-hydroxide for nucleophilic attack and facilitate proton transfer to Glu204. The resulting tetrahedral intermediate is stabilized by chelation to Co1 and by hydrogen-bonding interactions with His178 and His79. Proton transfer from Glu204 to the nitrogen atom of the scissile bond may facilitate breakdown of the intermediate to products. On the basis of the Met-eMetAP complex, collapse of the transition state to methionine results in the restoration of 5-fold coordination to Co1 while retaining the metal-bridging and His178 interactions. This is consistent with the spectroscopic analysis of wild-type and mutant eMetAPs (*17*). Regeneration of the active site for another round of catalysis occurs with the release of methionine and the deprotonation of solvent molecules. Some components of this scheme have been suggested for AMPP, although there are also some differences in the proposed interactions with the metal center (*19*).

The mechanism proposed for eMetAP has many similarities to those offered for other enzymes exhibiting mononuclear and dinuclear metal centers. In particular, the role of Glu204 as a proton shuttle is analogous to that proposed for Glu143 in thermolysin (*36*−*38*), Glu270 in carboxypeptidase (*39*), Glu383 in AMPP (*19*), Asp128 in arginase (*40*), Glu133 in peptide deformylase (*41*), and possibly Glu151 in *Aeromonas proteolytica* aminopeptidase (*42*, *43*).

The role of His178 may also be reminiscent of His141 and His64 in arginase and carbonic anhydrase II, respectively (*40*, *44*, *45*). His141 in arginase has been proposed to act as a proton shuttle to the leaving amino group. In a manner similar to His64 in carbonic anhydrase II, His141 may also expedite the formation of the nucleophile by providing a pathway for the release of a proton to solvent. In the resting state of eMetAP a water molecule hydrogen bonds between the metal-bridging hydroxide and His178 (*17*). This hydrogen-bonding network may facilitate the formation of the nucleophile during the regeneration step of the reaction cycle. The role of His178 is, however, not critical for catalysis as shown by the significant residual activity of the His178Ala mutant of eMetAP (*17*) and the His339Asn mutant of human MetAP−II (*11*). Interestingly, His178 in eMetAP is conserved in all MetAPs and AMPP, but is replaced in creatinase by Arg335 which forms a key salt bridge with the carboxylate of carbamyl sarcosine (*34*).

The importance of His79 in the mechanism of MetAPs is emphasized by the loss in activity of the His79Ala mutant of eMetAP (*17*) and the His231Asn mutant of hMetAP−II (*11*). Our previous determination of the bestatin-based inhibitor complex of eMetAP suggested that His79 might

interact with the carbonyl oxygen atom of the penultimate residue (*17*). The results presented herein, however, suggest that His79 may interact directly with the nitrogen of the scissile peptide bond. Such an interaction is more consistent with the cognate interactions observed in AMPP and creatinase as discussed above.

The need for such a backbone interaction may stem from the funnel-like nature of the active site which rapidly narrows from a wide mouth to a relatively narrow base where the methionine side chain binds. The substrate-like inhibitor complex shows that the third residue of the inhibitor is completely solvent accessible making no direct contact with the enzyme. In the absence of supplemental interactions in this region, the hydrogen bond provided by His79 may be especially important. This use of a conserved hydrogen bond to recognize only a small portion of a larger substrate is similar to that observed in peptide deformylase (*41*, *46*). Additional support for His79 acting as a primary binding determinant for substrates extends from studies showing that His79 and the structurally equivalent histidines in the yeast and human MetAPs are covalently modified by the natural product fumagillin and its derivatives (*9*−*13*). In these modification reactions, histidine probably acts as the attacking nucleophile on the ring epoxide group. The basicity of this histidine correlates well with the proposed role of His79 in the hydrolysis of substrates.

The conservation of the amino acid residues that generate the dinuclear metal center of MetAPs (*35*) emphasizes the key role the metal ions play in generating the nucleophile for catalysis. Moreover, the mutation of any of the metal ligands of eMetAP resulted in a marked reduction in activity and the loss of both metal ions (*47*). Activity has been observed for MetAPs substituted with Co(II), Mn(II), and Zn(II) (*1*, *17*, *48*−*50*) and with anaerobically Fe(II)-substituted eMetAP (*51*). It appears that the nature of the metal ion in the active site may influence or modulate the affinity for and turnover of substrates. Similar effects on catalysis have been observed for the structurally unrelated leucine aminopeptidase with different metal compositions (*52*). At this point it is unclear whether a change in metal composition of eMetAP would alter the binding mode of ligands to the metal center.

Accommodation within the S_1 Subsite. The present study shows that eMetAP is capable of binding not only methionine within the S_1 subsite, but also the nonnatural amino acid side chains of norleucine (Figure 2B) and trifluoromethionine (Figure 2E). Despite the substitution of the sulfur atom for carbon in NleP and the addition of three fluorines to the C^{ϵ} atom in TFM, the locations of these side chains within the S_1 subsite are very similar (Figure 4, panels A and B). The slight differences that are observed do not appear to affect the coordinating interactions at the metal center. This suggests that these and other synthetic analogues may be able to exploit improved shape complementarity to enhance the specific inhibition of eMetAP and other methionine aminopeptidases.

ACKNOWLEDGMENT

We thank Dr. Allen Orville for review of the manuscript and helpful discussions. We gratefully acknowledge Drs. L. Weaver, D. Tronrud, M. Quillin, M. Sagermann, I. Korndörfer, M. Elsliger and D. Juers for their assistance in all aspects of data collection, model building and refinement.

REFERENCES

1. Ben-Bassat, A., Bauer, K., Chang, S. Y., Myambo, K., Boosman, A., and Chang, S. (1987) *J. Bacteriol. 169*, 751−757.
2. Walker, K. W., and Bradshaw, R. A. (1999) *J. Biol. Chem. 274*, 13403−13409.
3. Bradshaw, R. A., Brickey, W. W., and Walker, K. W. (1998) *Trends Biochem. Sci. 23*, 263−267.
4. Arfin, S. M., and Bradshaw, R. A. (1988) *Biochemistry 27*, 7979−7984.
5. Meinnel, T., Mechulam, Y., and Blanquet, S. (1993) *Biochimie 75*, 1061−1075.
6. Chang, S. Y., McGary, E. C., and Chang, S. (1989) *J. Bacteriol. 171*, 4071−4072.
7. Miller, C. G., Kukral, A. M., Miller, J. L., and Movva, N. R. (1989) *J. Bacteriol. 171*, 5215−5217.
8. Li, X., and Chang, Y. H. (1995) *Proc. Natl. Acad. Sci. U.S.A. 92*, 12357−12361.
9. Lowther, W. T., McMillen, D. A., Orville, A. M., and Matthews, B. W. (1998) *Proc. Natl. Acad. Sci. U.S.A. 95*, 12153−12157.
10. Griffith, E. C., Su, Z., Turk, B. E., Chen, S., Chang, Y. H., Wu, Z., Biemann, K., and Liu, J. O. (1997) *Chem. Biol. 4*, 461−471.
11. Griffith, E. C., Zhuang, S., Niwayama, S., Ramsay, C. A., Chang, Y. H., and Liu, J. O. (1998) *Proc. Natl. Acad. Sci. U.S.A. 95*, 15183−15188.
12. Sin, N., Meng, L., Wang, M. Q., Wen, J. J., Bornmann, W. G., and Crews, C. M. (1997) *Proc. Natl. Acad. Sci. U.S.A. 94*, 6099−6103.
13. Liu, S., Widom, J., Kemp, C. W., Crews, C. M., and Clardy, J. (1998) *Science 282*, 1324−1327.
14. Folkman, J. (1995) *Nat. Med. 1*, 27−31.
15. Folkman, J. (1995) *N. Engl. J. Med. 333*, 1757−1763.
16. Roderick, S. L., and Matthews, B. W. (1993) *Biochemistry 32*, 3907−3912.
17. Lowther, W. T., Orville, A. M., Madden, D. T., Lim, S., Rich, D. H., and Matthews, B. W. (1999) *Biochemistry 38*, 7678−7688.
18. Schechter, I., and Berger, A. (1967) *Biochem. Biophys. Res. Commun. 27*, 157−162.
19. Wilce, M. C., Bond, C. S., Dixon, N. E., Freeman, H. C., Guss, J. M., Lilley, P. E., and Wilce, J. A. (1998) *Proc. Natl. Acad. Sci. U.S.A. 95*, 3472−3477.
20. Houston, M. E., and Honek, J. F. (1989) *J. Chem. Soc., Chem. Commun.* 761−762.
21. Duewel, H., Daub, E., Robinson, V., and Honek, J. F. (1997) *Biochemistry 36*, 3404−3416.
22. Kudzin, Z. H., and Stec, W. J. (1980) *Synthesis*, 1032−1034.
23. Bayliss, E. K., Campbell, C. D., and Dingwall, J. G. (1984) *J. Chem. Soc., Perkin Trans. 1*, 2845−2853.
24. Genet, J. P., Uziel, J., and Juge, S. (1988) *Tetrahedron Lett. 29*, 4559−4562.
25. Otwinowski, Z., and Minor, W. (1997) *Methods Enzymol. 276*, 307−326.
26. Sack, J. S., and Quiocho, F. A. (1997) *Methods Enzymol. 277*, 158−172.
27. Jones, T. A., and Kjeldgaard, M. (1997) *Methods Enzymol. 277*, 173−208.
28. Tronrud, D. E. (1997) *Methods Enzymol. 277*, 306−319.
29. Tronrud, D. E. (1996) *J. Appl. Crystallogr. 29*, 100−104.
30. Esnouf, R. M. (1997) *J. Mol. Graph. 15*, 132−138.
31. Kraulis, P. J. (1991) *J. Appl. Crystallogr. 24*, 946−950.
32. Keding, S. J., Dales, N. A., Lim, S., Beaulieu, D., and Rich, D. H. (1998) *Synth. Commun. 28*, 4463−4470.
33. Cunningham, D. F., and O'Connor, B. (1997) *Biochim. Biophys. Acta 1343*, 160−186.
34. Coll, M., Knof, S. H., Ohga, Y., Messerschmidt, A., Huber, R., Moellering, H., Russmann, L., and Schumacher, G. (1990) *J. Mol. Biol. 214*, 597−610.

35. Bazan, J. F., Weaver, L. H., Roderick, S. L., Huber, R., and Matthews, B. W. (1994) *Proc. Natl. Acad. Sci. U.S.A. 91*, 2473−2477.
36. Hangauer, D. G., Monzingo, A. F., and Matthews, B. W. (1984) *Biochemistry 23*, 5730−5741.
37. Monzingo, A. F., and Matthews, B. W. (1984) *Biochemistry 23*, 5724−5729.
38. Matthews, B. W. (1988) *Acc. Chem. Res. 21*, 333−340.
39. Christianson, D. W., and Lipscomb, W. (1989) *Acc. Chem. Res. 22*, 62−69.
40. Kanyo, Z. F., Scolnick, L. R., Ash, D. E., and Christianson, D. W. (1996) *Nature 383*, 554−557.
41. Hao, B., Gong, W., Rajagopalan, P. T., Zhou, Y., Pei, D., and Chan, M. K. (1999) *Biochemistry 38*, 4712−4719.
42. Chevrier, B., Schalk, C., D′Orchymont, H., Rondeau, J. M., Moras, D., and Tarnus, C. (1994) *Structure 2*, 283−291.
43. Chen, G., Edwards, T., D'souza V, M., and Holz, R. C. (1997) *Biochemistry 36*, 4278−4286.
44. Silverman, D. N., and Lindskog, S. (1988) *Acc. Chem. Res. 21*, 30−36.
45. Christianson, D. W., and Fierke, C. A. (1996) *Acc. Chem. Res. 29*, 331−339.
46. Becker, A., Schlichting, I., Kabsch, W., Groche, D., Schultz, S., and Wagner, A. F. (1998) *Nat. Struct. Biol. 5*, 1053−8.
47. Chiu, C., Lee, C., Lin, K., Tam, M. F., and Lin, L. (1999) *J. Bacteriol. 181*, 4686−4689.
48. Walker, K. W., and Bradshaw, R. A. (1998) *Protein Sci. 7*, 2684−2687.
49. Chang, Y. H., Teichert, U., and Smith, J. A. (1992) *J. Biol. Chem. 267*, 8007−8011.
50. Li, X., and Chang, Y. H. (1996) *Biochem. Biophys. Res. Commun. 227*, 152−159.
51. D'souza, V. M., and Holz, R. C. (1999) *Biochemistry 38*, 11079−11085.
52. Allen, M. P., Yamada, A. H., and Carpenter, F. H. (1983) *Biochemistry 22*, 3778−3783.

BI991711G